Journal of Nuclear Materials 462 (2015) 374–381

Contents lists available at ScienceDirect

Journal of Nuclear Materials

journal homepage: www.elsevier.com/locate/jnucmat

Small-scale characterisation of irradiated nuclear materials: Part II nanoindentation and micro-cantilever testing of ion irradiated nuclear materials

D.E.J. Armstrong [a,*], C.D. Hardie [a,b], J.S.K.L. Gibson [a], A.J. Bushby [c], P.D. Edmondson [a], S.G. Roberts [a,b]

[a] Department of Materials, University of Oxford, Oxdord OX1 3PH, United Kingdom
[b] EURATOM/CCFE Association, Culham Centre for Fusion Energy (CCFE), Abingdon, Oxfordshire OX14 3DB, United Kingdom
[c] School of Engineering and Materials Science, Queen Mary University of London, Mile End Road, London E1 4NS, United Kingdom

ARTICLE INFO

Article history:
Available online 30 January 2015

ABSTRACT

This paper demonstrates the ability of advanced micro-mechanical testing methods, based on FIB machined micro-cantilevers, to measure the mechanical properties of ion implanted layers without the influence of underlying unimplanted material. The first section describes a study of iron–12 wt% chromium alloy implanted with iron ions. It is shown that by careful cantilever design and finite element modelling that changes in yield stress after implantation can be measured even with the influence of a strong size effect. The second section describes a study of tungsten implanted with both tungsten ions and tungsten and helium ions using spherical and sharp nanoindentation, and micro-cantilevers. The spherical indentation allows yield properties and work hardening behaviour of the implanted layers to be measured. However the brittle nature of the implanted tungsten is only revealed when using micro-cantilevers. This demonstrates that when applying micro-mechanical methods to ion implanted layers care is needed to understand the nature of size effects, careful modelling of experimental procedure is required and multiple experimental techniques are needed to allow the maximum amount of mechanical behaviour information to be collected.

1. Introduction

For the successful development and deployment of advanced nuclear reactors such as GEN IV fission types and fusion devices such as tokamaks or inertial confinement devices, there is a vital need to understand the effect of radiation damage from neutrons and charged particles on the mechanical properties of structural materials [1–4]. While some work can, and indeed must, be carried out on neutron irradiated samples, ideally irradiated at conditions as close to those seen in service as possible, this approach suffers from several difficulties. Firstly the neutron irradiated samples are by their nature active and must be handled with care and tested in hot cells. Secondly the cost and timescale over which such irradiation campaigns take place limit the number of variables which can be studied, and preclude rapid response to results. Finally there is no available source of 14 MeV neutrons, with sufficient flux to mimic fusion environments. Ion implantation can fill the gap here, allowing high damage levels to be produced quickly and comparably cheaply.

The use of ion implantation to study radiation damage and mimic neutron damage has a long history [5]. Transmission electron microscopy (TEM) has been widely used both with in-situ ion beams to study the formation of damage structures during irradiation and post implantation to study the final damage networks formed [6,7]. Alongside this, field ion microscopy and atom probe tomography have been used to investigate the damage formation and the chemical changes which can occur during irradiation [8,9]. These are further discussed in the paper of Edmondson et al. in this edition. [10]. The ability to measure the mechanical properties of ion implanted structures has lagged behind, due to the difficulties associated with measuring the mechanical properties of such thin layers (typically ~0.2 to 2 μm deep) and then in relating them to macroscopic mechanical properties. Most of the work thus far has used micro and nano-indentation techniques to probe the mechanical properties of these layers. This comes with inherent difficulties. Firstly the hardness is not a fundamental mechanical property and different testing techniques can give different "hardness values" on nominally the same material [11]. Much work has been carried out using finite element and other empirical techniques to extract a yield or flow stress from indentation data, but due to the complex and ill-defined stress state no

* Corresponding author.
E-mail address: david.armstrong@materials.ox.ac.uk (D.E.J. Armstrong).

http://dx.doi.org/10.1016/j.jnucmat.2015.01.053
0022-3115/

general method has been developed [12]. Secondly the ion implanted layers are nearly always on top of an unimplanted bulk material and deconvoluting the influence of this layer on the measured mechanical properties is difficult, particularly if the exact damage profile from implantation is unknown [13–16]. While methods used for analysing coating systems and their substrates can be used, the situation is more complex as the implanted layers vary in structure with depth and there is no longer a sharp boundary between the surface layer and substrate. Nonetheless indentation is an important tool in comparing implanted and unimplanted samples due to its comparative ease and speed of use and its ability to give quantitative data. A fuller discussion of indentation of irradiated layers can be found in the paper by Hardie et al. [17] in this special edition.

Development of micro-scale manufacturing methods such as focused ion beam machining, together with advances in indentation instrumentation, has allowed the manufacture and testing of micro-scale mechanical test structures with well-defined stress states, typically micro-pillars or micro-cantilevers. These have allowed measurement of basic mechanical properties such as elastic modulus [18,19], yield stress [20–24] and fracture properties [25–28], which are key parameters in engineering design. Either by manufacturing micro-scale test structures and then ion implanting them or by manufacturing the test pieces into pre-implanted layers it is possible to directly measure the mechanical properties of the damaged region without influence of the underlying material.

Pillars are the most widely used FIB machined micro- and nano-mechanical testing geometry used, due to their relative ease of manufacture and apparently simple stress state of uniaxial compression. Micropillars have been used in several studies of irradiated materials. Kiener et al. [29] produced pillars with diameters from 80 nm to 1500 nm in copper, irradiated to 0.8 dpa using protons, which were then compressed inside a TEM. They observed an increase of ≈100–250 MPa in yield stress for irradiated vs non-irradiated samples above 400 nm diameter; however, below 400 nm diameter, no difference between irradiated and unirradiated pillars was seen. This work allowed the deformation mechanisms to be observed directly but only allows small pillars (thin enough to be electron transparent) to be tested. Grieveson et al. [30] used 1 μm diameter micropillars to study the yield properties of pure iron in both the unimplanted state and self-ion-implanted to 6 dpa. While nanoindentation showed a clear increase in hardness in the implanted region, no significant change in the yield stress of the micro-pillars after irradiation was observed. Post-test examination showed that the unimplanted pillars failed by a giant shear type mechanism as commonly seen in other single crystal micro-pillars, while the failure of the implanted pillars was seen to be by multiple slip events on a stack of closely-spaced parallel slip planes. These differences in deformation behaviour were also apparent in the stress–strain curves, with the unimplanted material deforming by a small number of large strain jumps, and the implanted material by a larger number of smaller strain jumps. This was attributed to differences in behaviour of dislocations produced by the small number of dislocation sources in both sets of pillars. In the unimplanted pillars once the dislocation source is activated slip continues until it exits the pillar, producing a few discrete slip steps each with large associated strain, as has been commonly found in micro pillar deformation [24]. However the radiation damage in the implanted pillar acts as a dense distribution of obstacles to dislocation motion. Three mechanisms – cross-slip, stress concentrations due to pile up and stress-concentrations due to shear channels were suggested as reasons for the different flow behaviour in implanted micropillars.

The work by Grieveson et al. [30] also demonstrates one of the commonly seen weaknesses of micro-pillars in that an appreciable taper is seen on the pillars when produced by annular milling. This results in a more complex stress state making quantitative analysis of elastic modulus and yield stress difficult. Copper pillars have been manufactured by Gue et al. [31] using templating and electroplating. This allowed pillars of diameter 100–400 nm to be manufactured with no ion damage from FIB machining, and with a more uniform cross section than by FIB machining. After manufacture these pillars were then implanted with helium ions to a damage level of 0.7 dpa with a calculated helium concentration of 0.35 at.%. Although the 125 nm pillar showed little change in yield stress after irradiation, an increase in yield stress was observed in the 400 nm pillar; this contrasts with the work of Kiener et al. [29] who observed no increase in strength of <400 nm diameter copper pillars irradiated with protons. Gue et al. also saw a transition similar to that seen by Grieveson [30], where multiple short strain bursts occurred during compression after irradiation compared to fewer larger strain bursts in unirradiated material. Additionally they saw an increase in work hardening rate in irradiated material.

Halliday et al. [32] used nanoindentation and "waisted" micro-cantilever tests to measure the hardness and yield stress of a range of Fe–*X* wt%Cr alloys (where X ranges from 0% to 12%). Indentation tests showed an increase in hardness in all implanted alloys, but a significant effect from the underlying unimplanted material could be seen in hardness–displacement data. Analysis of tests on waisted micro-cantilevers, using simple elastic beam theory, showed that the yield stress in the implanted material increased only slightly on implantation to 0.35 dpa, but on implantation to 5.33 dpa both modulus and hardness significantly increased. The modulus of this heavily irradiated material, 374 GPa, is over a 100 GPa higher than that generally reported for pure iron. It seems likely that this is due to inaccuracies in either the measuring or manufacture of the waisted micro-cantilever and to the simplistic simple beam type analysis used; and as such is not thought to be physically realistic. This clearly demonstrates the need for accurate cantilever design, measurement and modelling if reliable stress–strain data is to be obtained.

Thus it is clear that while micromechanical testing techniques potentially offer considerable advantages over indentation methods for mechanical characterisation of ion implanted layers, this potential cannot be exploited without a better understanding of the deformation processes occurring during such tests, and without reliable techniques for analysis of micromechanical test data. Establishing that understanding and these techniques is an ongoing research effort; in this paper we will demonstrate the use of micro-mechanical testing techniques on two very different materials systems subjected to very different irradiation conditions, leading to the determination of mechanical data not possible using nanoindentation experiments alone.

2. Experimental work

In Part 1 an iron 12 wt% chromium alloy, the basis for a large number of nuclear ferritic alloys, is subjected to 2 MeV Fe+ ion implantation at 320 °C to a damage level of 6 dpa to act as an analogue of the damage produced by neutrons in an advanced fission or fusion reactor. In Part 2 tungsten samples are implanted with W^+ ions, and W^+ and He^+ ions simultaneously at 800 °C, giving damage levels of 1 dpa and 650 appm helium. This acts as an analogue for both the neutron and helium irradiation that a tungsten alloy will undergo in both structural and plasma facing rolls in future nuclear fusion reactors such as DEMO [33,34]. In both cases micro-cantilever bending and nanoindentation experiments were used to study the changes in the mechanical behaviour of these ion implanted layers. Use of these two rather different metals illustrates the utility of micromechanical test methods for study

of irradiation effects on mechanical behaviour for materials ranging from a metal with a moderate yield strength but high toughness and work-hardening capacity (Fe–Cr) to one with very high strength but low toughness (W).

2.1. Part1: Elastic and plastic properties of self-ion implanted Fe12Cr

Due to high fracture toughness, and high temperature strength steel has served the nuclear industry for decades as a robust, structural material for reactor pressure vessels (RPV). Ferritic/martensitic steels containing ~9% to 15%Cr are promising candidates for structural components in both Gen IV fission reactors [4] and future fusion devices [35] due to their superior resistance to swelling and irradiation embrittlement. The analysis of data from several RPV steels has identified that irradiation hardening of these materials exhibits a strong non-monotonic dependence on Cr content [36,37] and exhibits a minimum irradiation-induced increase in the ductile to brittle transition temperature (DBTT) in alloys containing 9%Cr [38]. In order to further understand and develop these steels, there is increasing interest in the effects of Cr on the effects of irradiation, using binary Fe–Cr alloys as model materials. This section reports on micro-cantilever techniques used to measure the mechanical properties of Fe12%Cr subject to ion implantation.

The material, sample preparation and irradiation conditions are as reported Hardie and Roberts [16]. Ultra High Purity (99.999%) polycrystalline Fe12%Cr was produced in the form of sheet by 'Metals, Crystals and Oxides Limited' (Cambridge, UK). The material was annealed at 830 °C for 72 h in vacuum to remove cold work deformation arising from the materials manufacture. The samples were lapped and polished using a series of diamond pastes, followed by a chemo-mechanical polish using a colloidal silica suspension to remove polishing damage from previous steps. The average grain size as analysed by Electron Back Scattered Diffraction (EBSD) on these well-polished surfaces was ≈190 μm.

Ion implantation of the material took place at the Surrey Ion Beam Centre (UK). The Monte Carlo code TRIM [39] was used in pure iron with the recommended displacement energy of 40 eV [ASTM Standard, ASTM E521-96(2009) (2009)] to design the beam conditions. Fe^{+} ions were implanted with energies of 2 MeV (3×10^{15} ions cm^{-2}) and subsequently 0.5 MeV (1.5×10^{15} ions cm^{-2}) to produce a damage profile with depth of ≈800 nm and with an average of damage level of 6.18 dpa, as shown in Fig. 1. A cross-sectional TEM micrograph of the damage distribution with depth is shown in Fig. 2 for comparison. The implantation took place at a constant temperature of 320 °C with an average dose rate of 5×10^{-4} dpa s^{-1}. Nanoindentation results for this

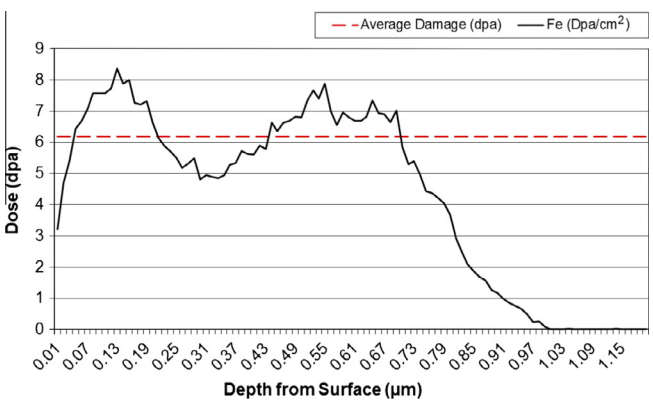

Fig. 1. Distribution of damage with depth into sample surface. Calculations performed using TRIM with a displacement energy of 40 eV for iron.

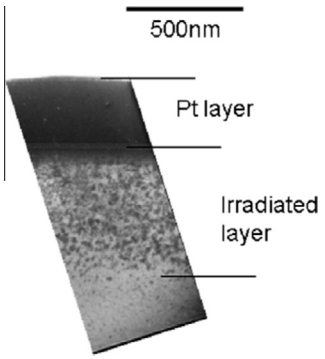

Fig. 2. TEM cross-sectional micrograph of the irradiated layer in Fe12%Cr.

Fe12Cr alloy have already been reported by Hardie and Roberts [16] and Hardie et al. [17]. The hardness in the implanted region increases by ≈1 GPa after implantation to 6.18 dpa as measured using Berkovich indentation.

After implantation, the region of the sample exposed to the beam was clearly visible in secondary electron images produced in the SEM/FIB, by a difference in contrast with the rest of the sample. This enabled the FIB milling of marker lines, visible under an optical microscope, at the implanted/un-implanted boundary thus assisting manufacture of micro-cantilever testing elements in implanted and un-implanted regions within same grain. Two designs of cantilevers were manufactured using FIB machining: A simple micro-cantilever with triangular, uniform cross-section (Fig. 3a) and a waisted cantilever with gauge section at the base for controlling the distribution of plastic deformation (Fig. 3b). For each beam type, arrays of 12 beams were manufactured in the un-irradiated and ion-irradiated regions of the same grain. Arrays with example beams are shown in Fig. 3. For a full discussion of micro-cantilever manufacture methods see [19,25].

All beams were measured by SEM-based photogrammetric methods as described in [40]. Each beam was viewed at tilt angles of 39° and 63° and at a working distance of approximately 10 mm. These measurements were required for measuring the gauge geometry in the waisted beams, where the relevant cross-section was not visible, and benefited from higher accuracy because they were independent of sample orientation with respect to the SEM column.

Loading of the both the triangular and waisted micro-cantilevers was performed using a Nano Indenter-XP (MTS, TN, USA) instrument, with a Berkovich tip. The triangular cantilever tests were loaded with a target final strain of 0.05 and strain rate of 2×10^{-4} s^{-1} (in both cases at the cantilever root lower surface), which required total displacements ranging from 700 to 1200 nm and constant displacement rates of 2.9–4.5 nm s^{-1}, according to simple beam theory calculations. The waisted beams were loaded with a constant displacement rate of 5 nm s^{-1}. Maximum loads during testing were in the region of 20–30 μN, which was not sufficient to leave a visible impression into the surface with the Berkovich tip. The location of the point of loading (where the indenter tip and beam made contact) was observable by a faint contrast mark using the in-lens secondary electron detector in the SEM. As with the beam measurements, the position of this with respect to the free end of the beam was measured by photogrammetric methods.

Typical maximum stress–maximum strain curves for tests on triangular in the irradiated and un-irradiated materials are shown in Fig. 4. The un-irradiated beams exhibited several load drops during plastic deformation. These load drops are not apparent in the irradiated material. Average mechanical property measurements made

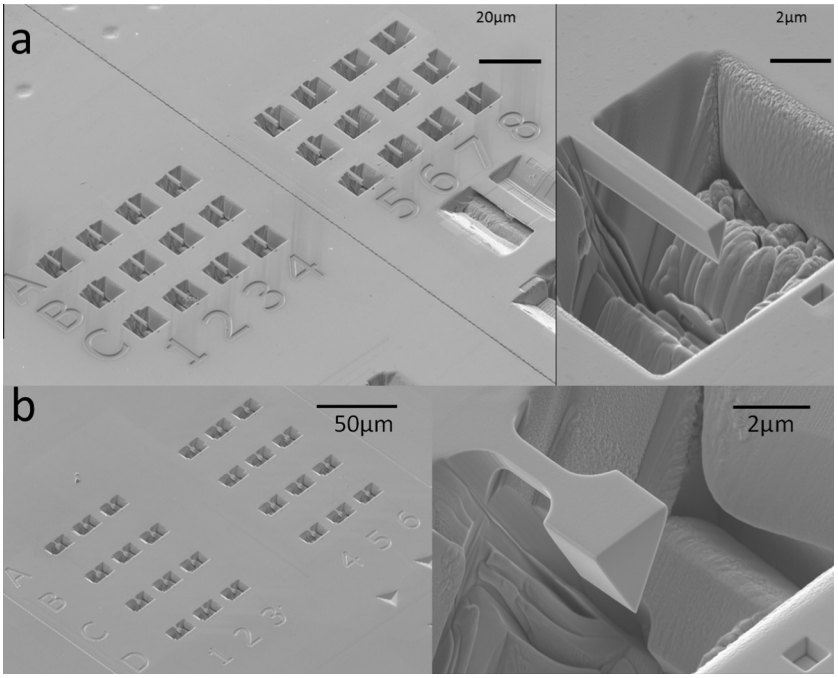

Fig. 3. SEM images of arrays and typical micro-cantilevers with (a) a uniform cross-section and (b) waisted section.

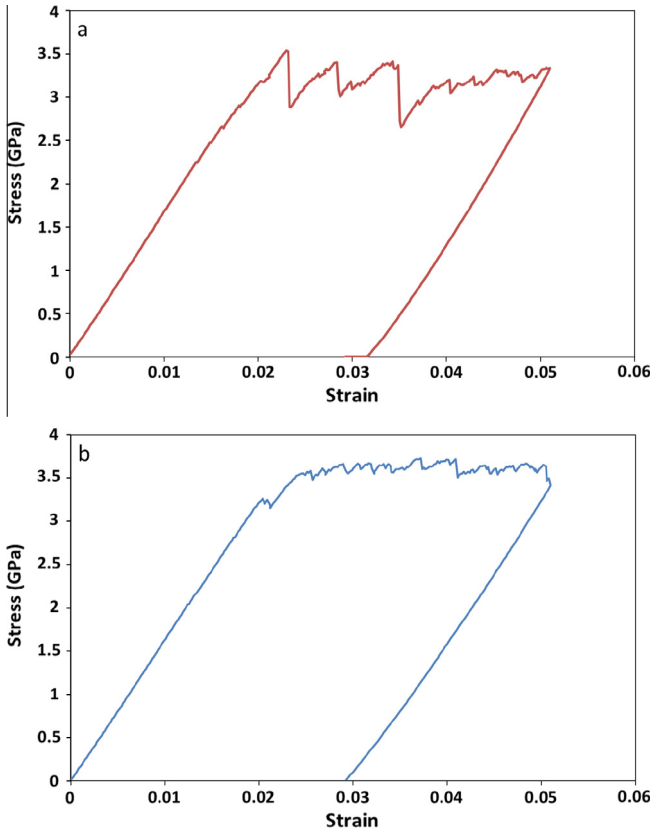

Fig. 4. Typical maximum stress–maximum strain curves for triangular Fe12%Cr micro-cantilevers in (a) unimplanted and (b) implanted condition.

Table 1
Average mechanical property measurements produced by FEA analysis for both cantilever types in un-irradiated and irradiated Fe12%Cr.

	Un-irradiated			Irradiated		
		SD	%		SD	%
Uniform cross-section						
Elastic modulus (GPa)	205	14	6.7	195	30	15.4
Yield stress (GPa)	1.8	0.3	17.6	1.7	0.2	9.6
Waisted beam						
Elastic modulus (GPa)	277	26	9.5	299	50	16.9
Yield stress (GPa)	1.6	0.1	3.8	2.1	0.4	22.2

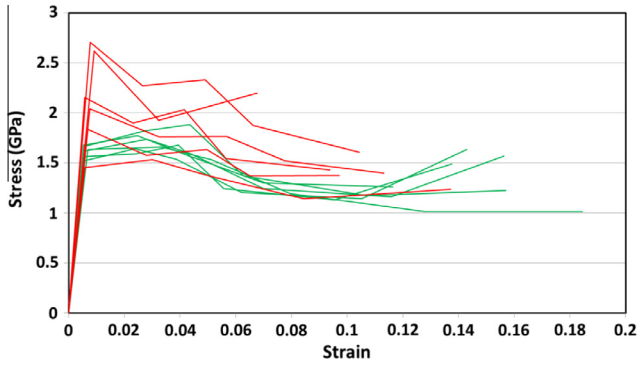

Fig. 5. Matched model stress–strain curves for 'waisted' type beams tested in the un-irradiated (shown in green) and irradiated (shown in red) regions of Fe 12%Cr. (For interpretation of the references to colour in this figure legend, the reader is referred to the web version of this article.)

using beams of both designs from both irradiated and un-irradiated regions of the sample are shown in Table 1.

For both cantilever geometries FEA analysis was used to fit the experimental data for each test, via a process of progressive convergent approximation to convert load–displacement data into a stress–strain curve. For each beam, this involved several tens of simulations for an accurate fit. A series of analysis tools was written in MATLAB for automation of experimental data interpretation by the iterative FEA simulations. Typical data for waisted micro-cantilevers is shown in Fig. 5.

The difference in elastic modulus as measured by the different beam types is likely to be due to differing crystallographic orientations between the beam types, which were made in different grains. The elastic anisotropy of pure iron results in a modulus range of ≈150 GPa along the ⟨100⟩ axis to ≈270 GPa along ⟨111⟩ axis [41], therefore the measurements of elastic modulus for the two beam types are within the expected range for the Fe12%Cr alloy; within the experimental accuracy no changes in elastic modulus are observed due to implantation.

For the triangular beams (uniform cross section) there is no significant change in the yield stress after irradiation (1.8 GPa unirradiated; 1.7 GPa irradiated). The FEA analysis on the complex beam geometry shows a significant increase in average yield stress, from 1.6 GPa in the unirradiated condition to 2.1 GPa after irradiation. This is in good agreement with the hardness data on the same sample in Hardie et al. [16] which shows a hardness increase of ≈1.1 GPa measured using nanoindentation.

As the yield stress measured using microcantilevers is greater than 1.5 GPa in the un-irradiated material, compared to 300 MPa for tensile tests on bulk samples of Fe12Cr [42], it is obvious that all these micro-cantilever test are strongly influenced by the well-established size effect, where smaller specimens show very increased flow stresses. This effect has been attributed in micropillar testing to the small number and small size of potential dislocation sources, and to their rapid "exhaustion" during deformation [24]. However, in micro-cantilever tests, unlike compression tests, the volume subjected to the maximum stress is not static. As the bending moment is increased the volume at maximum stress grows. In the case of both designs of micro-cantilever here the maximum stress is on the underside of the beam close to the fixed end. However, for the waisted micro-cantilever, the region being subjected to the peak stress is ≈20 larger than in the simple triangular cantilever, as shown in Fig. 6. As such the stochastic nature of the deformation dominates in the triangular cantilevers with a much smaller stressed region; whereas in the waisted cantilevers the increased highly stressed volume increases the chance a dislocation source is present – resulting in a lower yield stress in the unirradiated condition compared to triangular micro-cantilevers in the same condition even though the physical size of the cantilever is smaller. Due to the very small size of the stressed region in the triangular cantilevers after implantation there is no observed change in yield stress as this is still controlled by activation of single sources within this small volume. However the activation of sources in the waisted cantilevers is easier and large load drops are not observed. Thus the yield stress is controlled by the interaction of mobile dislocations with the damage from the ion implantation. This is in agreement with work by Kiener et al. [29] who did not observe increases in yield stress for proton irradiated Cu micropillars of diameter less than 400 nm but did see increases in yield stress in larger pillars.

2.2. Part 2: plastic deformation and fracture in helium and tungsten implanted tungsten

2.2.1. Introduction

Tungsten is the most attractive material for use in plasma facing components of nuclear fusion reactors due to its combination of high melting point, high thermal conductivity, resistance to sputtering erosion and low level of activation. However its mechanical behaviour after irradiation, which is key engineering design data which is required for future fusion reactors [43], is not well characterised.

2.2.2. Experimental methods

Two different grades of tungsten were implanted: ultra-high purity (UHP) tungsten (Plansee Austria), as used by Armstrong et al. [8] in previous self-ion implantation studies; and polycrystalline tungsten from Metals Crystal and Oxides Limited (Cambridge, UK) (MCO), previously used for study of brittle–ductile transition behaviour [44]. The UHP-W was annealed for 24 h at 1400 °C in vacuum, which produced a grain size ≈100 μm as measured using EBSD. The MCO-W was used in the as-received condition, as in the macro-scale DBTT studies, with a grain size of ≈2 μm as measured using EBSD. Both materials were prepared for implantation by chemo-mechanical polishing using colloidal silica; full methods are described in detail elsewhere [8].

For implantation, samples were mounted in a stainless steel holder with part of each sample blanked off to shield it from the ion beam, allowing testing of unimplanted material subjected to the same thermal treatment. Ion implantation was carried out at the JANNuS facility (Joint Accelerators for Nano and Nuclear Science) at CEA Saclay, France. He^{+} ions at 2 MeV and W^{12+} ions at

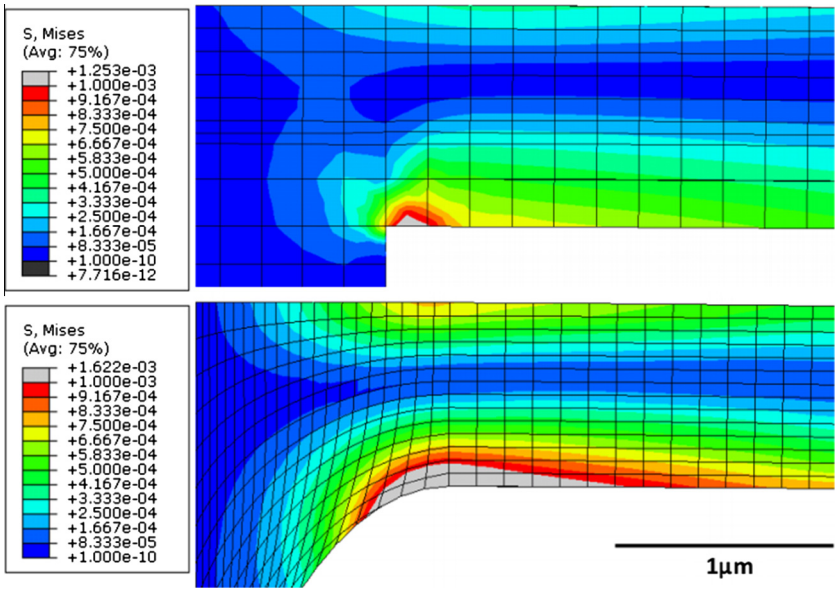

Fig. 6. Von Mises stress distribution in (a) triangular and (b) waisted micro-cantilevers. The peak stressed region is ≈20 larger in the waisted micro-cantilever.

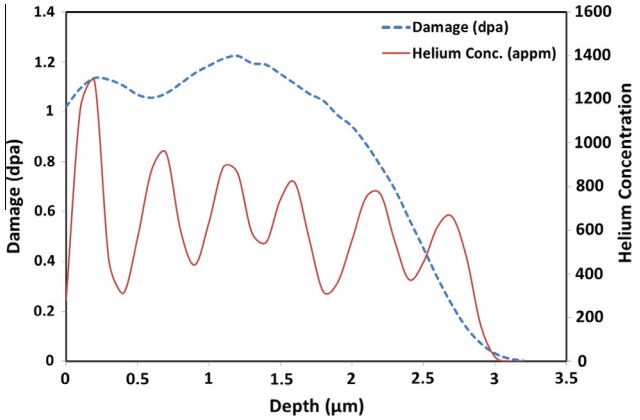

Fig. 7. Helium concentration and dpa distribution for dual-beam implanted tungsten. The dpa distribution is identical for W-ion implanted tungsten.

9 MeV were implanted. 1×10^{16} He ions cm^{-2} and 5×10^{14} W ions cm^{-2} were simultaneously implanted at a dose rate of 5.2×10^{-5} dpa s^{-1} and a temperature of 800 °C. To produce a 'flat' damage profile, the ion beams were passed through aluminium degrader foils in a rotating cassette of thicknesses 6, 5, 4, 3 and 1.6 μm, in addition to the un-degraded beam. A separate single-beam W-ion implantation was also carried out with the same energy, dose, dose rate and temperature. Due to the minimal damage from the helium ions, the damage (dpa) distribution for this single-beam implantation is effectively the same as in Fig. 7.

2.2.3. Nanoindentation experiments

Nanoindentation experiments were carried out using both a sharp Berkovich tip and a spherical tip. Berkovich indentations were made using a NanoIndenter XP (MTS, TN, USA) using the continuous stiffness measurement technique (with a 2 nm amplitude at 45 Hz). Indents were made to a depth of 2000 nm using a target strain rate of 0.05 s^{-1}. Spherical indentations were made using a UMIS 2000 (CSIRO, Lindfield, NSW, Australia) using a 5 μm radius indenter to a maximum load of 50 mN. The partial unload method (to 0.25 maximum load) was used to produce a profile of mechanical properties through the implanted layer. 50 indentations were made in each material condition, spaced by 50 μm to ensure that the plastic zones from individual indentations did not overlap.

Fig. 8 and Table 2 show the hardness as a function of depth and average hardness (100–500 nm) for Berkovich indentations made into the three material conditions (Unimplanted, W ion implanted and W ion and He ion implanted). The hardness of both implanted materials is significantly greater than that of the unimplanted material (≈6 GPa at 250 nm depth), with the dual ion implanted material being ≈2 GPa harder than the W ion implanted sample at 250 nm. The influence that that the unimplanted substrate material has on the indentation response is also evident in Fig. 8. Although the implanted region for both single and double ion implantation extends to 3 μm depth (Fig. 6), at 2 μm indenter depth in the implanted material the hardness data are dominated by the under lying material, and tend towards the unimplanted hardness value. This indicates that, as expected, the depth of the plastic zone associated with the indentations, which determines the hardness response, is considerably deeper that the indentation itself.

Spherical indentations were made to a maximum load of 50 mN; this gives a typical indentation depth of 250–300 nm. This ensured that the data were representative of the implanted layer and not unduly influenced by the underlying unimplanted material. Indentation stress–strain curves (mean contact pressure – contact radius/indenter radius) derived from the load – partial unload data, for the three material conditions are shown in Fig. 9 and average data are shown in Table 2. The data from the unimplanted material show a large elastic region before a large load drop associated with a "pop-in" event. A small load drop event is also visible in the W ion implanted sample; no pop-in is visible in the dual ion implanted material. Compared to Berkovich indentation, the spherical indentation allows analysis of both the yield stress and work hardening characteristics. The yield stress was cal-

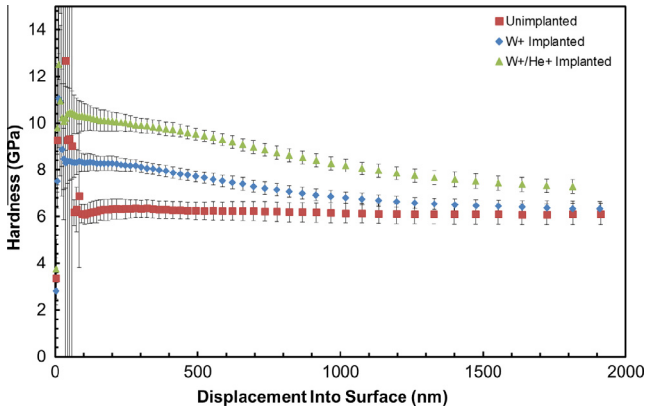

Fig. 8. Hardness–displacement curves for Berkovich nanoindentation using CSM in UHP-tungsten in all three conditions.

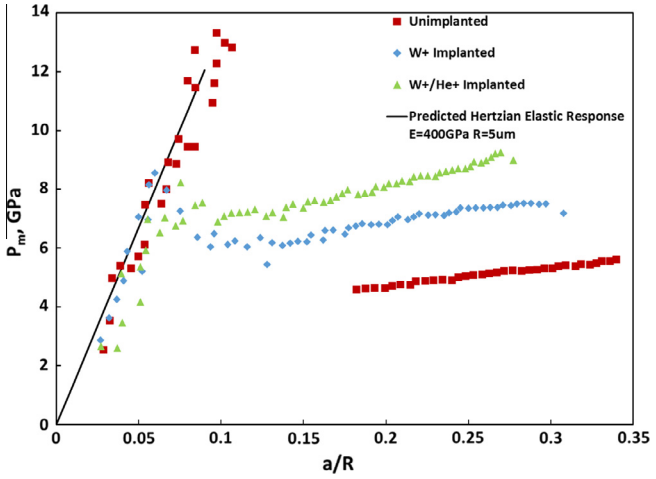

Fig. 9. Indentation stress–strain curves from spherical indentation for typical indentations for each UHP-W material condition. The solid line shows the predicted Herztian elastic response for a material of $E = 400$ GPa.

Table 2
Indentation data (Berkovich and Spherical) for UHP-tungsten.

	Unimplanted	W+ implanted	W + He+ implanted
Berkovich hardness (average 100–500 nm) (Gpa)	6.1	8.2	10.1
Average pop in stress (spherical indentation) (GPa)	9 ± 3.5	8.3 ± 1.9	–
Average yield stress (spherical indentation) (GPa)	4.1 ± 0.6	5.9 ± 0.7	6.6 + 0.6
Average work hardening (spherical indentation) coefficient	0.33 ± 0.07	0.20 ± 0.1	0.41 ± 0.09

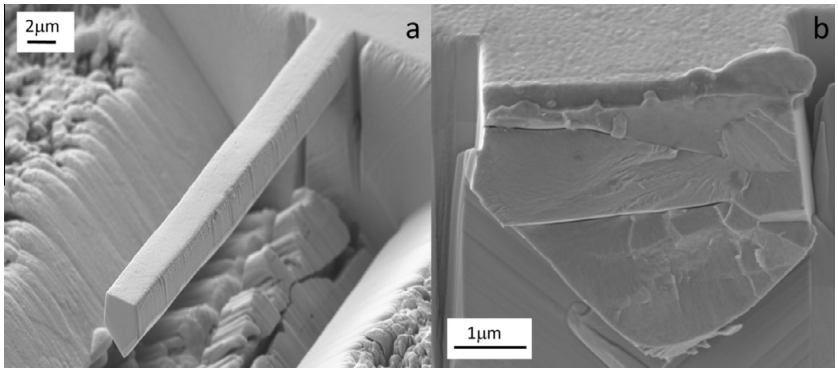

Fig. 10. (a) Pentagonal cantilever for fracture experiment pre-test. (b) Fracture surface after testing.

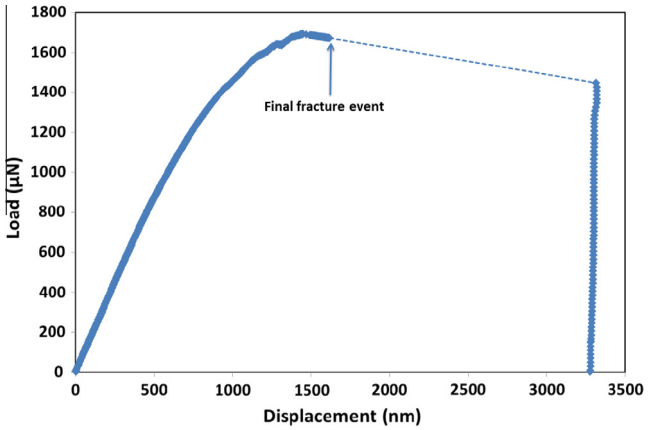

Fig. 11. Typical load–displacement curve for fractured tungsten cantilever with pentagonal cross section.

culated using the method of Bushby et al. [45]. For tests which exhibited a pop-in, extrapolating back from the flow portion of the stress–strain curve to the elastic portion allowed a yield point to be defined. The yield stress increases with irradiation, with a similar ratio as that by which the hardness increases due to irradiation in the Berkovich indentation tests. The average work hardening coefficient is seen to decrease after single ion irradiation, from 0.33 to 0.2, but increases after dual ion irradiation. This is likely to reflect changes in the type of irradiation defects; it is probable that in the dual-irradiated material there is a significant population of He-vacancy complexes [46], compared to dislocation loop damage in the W-irradiated material [7]. This is currently the subject of further investigation.

2.2.4. Fracture behaviour: Micro-cantilever tests

To investigate the fracture behaviour of the ion implanted tungsten, notched pentagonal micro-cantilevers (as previously used by Di Miao and Roberts [26]) were manufactured. A typical cantilever is shown in Fig. 10a. The beams were notched using a beam current of 10 pA for 10 s. The depth of the notch, required for calculation of fracture toughness, K_{1c}, was calculated from the fracture surface of each cantilever. In all cases cantilevers were loaded at 5 nm s^{-1} to a displacement of 2 μm; a typical load displacement curve is shown in Fig. 11 with the fracture event marked. For the notched pentagonal cantilevers, K_{1c} is given by Eq. (1) [26]:

$$K_{1c} = \frac{PLy\sqrt{\pi a}F\left(\frac{a}{b}\right)}{I} \quad (1)$$

where P is the applied bending force; L is the distance between the notch and the applied force; a is the notch depth, b is the depth of the cantilever and y, I and $F(a/b)$ are geometrical factors, calculated by Di Maio and Roberts [26] for pentagonal micro cantilevers.

Table 3 shows the calculated fracture toughness values for tungsten in each irradiation condition. No cantilevers fractured in the unimplanted or the W-ion implanted material. By taking the load at which the cantilever yielded as the 'failure load' and using this as the value of P in Eq. (1), a lower bound of fracture toughness can be determined. It can be seen that the tungsten implanted with helium and tungsten ions is more brittle as exhibited by fracture of two cantilevers. A fracture surface is shown in Fig. 10b. Whether this fracture is due to embrittlement of the tungsten by helium is unclear as only a small number of tests have been performed. However SEM examination of nanoindentations in all three material conditions showed no cracking or fracture events. This demonstrates the utility of micro-mechanical tests in measuring the micro-fracture properties of ion-implanted layers, which if only studied by indentation would not be observed. Further work is now ongoing in this area to fully characterise the effects of irradiation on fracture behaviour and embrittlement in tungsten.

3. Summary and conclusions

The results reported here show the power of nano and micro-scale mechanical testing techniques, especially when several complementary techniques are used in parallel, for understanding strength, deformation and failure of ion implanted layers. Several conclusions can be drawn.

(1) Indentation experiments provide a fast and easy method of evaluating the yield and flow behaviour of implanted layers. Care is needed in choice of indentation load/depth to ensure that the results are not unduly influenced by the unimplanted

Table 3
Average fracture toughness for tungsten micro-cantilevers.

Implantation condition	Unimplanted	Tungsten-ion implanted	Tungsten and helium-ion implanted
No. cantilevers tested	6	16	14
No. cantilevers fractured	0	0	2
Average fracture toughness	>10.1 MPa $\sqrt{m}$	>6.0 MPa $\sqrt{m}$	4.8 MPa $\sqrt{m}$

substrate; however, tests must cover a range of depths sufficient to characterise and account for indentation size effects.
(2) By using multiple tip geometries (in this case spherical and Berkovich) the maximum information from indentation experiments can be extracted, including work hardening behaviour and yield stress.
(3) Analysis of plastic deformation of micro-cantilevers produced wholly in implanted layers is complicated by the influence of geometry-based size effects. This can obscure changes in strength which are evident in indentation experiments.
(4) With careful design and manufacture of microcantilever, and use of iteratively fitted finite element analyses, the yield strength of implanted layers can be characterised and distinguished from that of unimplanted material.
(5) Fracture behaviour in radiation-embrittled layers can be studied and quantified using micro-cantilevers. Fracture behaviour of even very brittle irradiated metals cannot be studied by indentation methods on this scale.

When designing and implementing micro- and nano-mechanical studies of radiation damage, care must be taken to choose appropriate combinations of testing methods to study the effects of damage of interest. When taken individually the results of such tests are likely to give incomplete or misleading results, as seen in the embrittlement of tungsten, which is not revealed by indentation but only by bending experiments. The best results are obtained when several complementary techniques are used together.

Acknowledgements

DEJA thanks Culham Centre for Fusion Energy for funding via a Research Fellowship at St Edmund Hall, Oxford, and The Royal Academy of Engineering for a Research Fellowship at the University of Oxford. DEJA, JG, CDH, PDE and SGR acknowledge support from EPSRC Grants EP/H018921/1, EP/G004676/1, and EP/F004451/1, and the support of staff at the National Ion Beam Centre, University of Surrey, UK and at JANNuS CEA Saclay.

References

[1] B. Raj, M. Vijayalakshmi, P.R.V. Rao, K.B.S. Rao, MRS Bull. 33 (2008) 327–337.
[2] S.J. Zinkle, Epj Web Conf. 51 (2013).
[3] S.J. Zinkle, G.S. Was, Acta Mater. 61 (2013) 735–758.
[4] K.L. Murty, I. Charit, J. Nucl. Mater. 383 (2008) 189–195.
[5] G.S. Was, Fundamentals of radiation Materials Science: Metals and Alloys, Springer, Berlin, New York, 2007.
[6] M.M. Li, M.A. Kirk, P.M. Baldo, D.H. Xu, B.D. Wirth, Phil. Mag. 92 (2012) 2048–2078.
[7] X. Yi, M.L. Jenkins, M. Briceno, S.G. Roberts, Z. Zhou, M.A. Kirk, Philos. Mag. 93 (14) (2013).
[8] D.E.J. Armstrong, X. Yi, E.A. Marquis, S.G. Roberts, J. Nucl. Mater. 432 (2013) 428–436.
[9] E.A. Marquis, J.M. Hyde, D.W. Saxey, S. Lozano-Perez, V. de Castro, D. Hudson, C.A. Williams, S. Humphry-Baker, G.D.W. Smith, Mater. Today 12 (2009) 30–37.
[10] P.D. Edmondson, A. London, A. Xu, D.E.J. Armstrong, S.G. Roberts, J. Nucl. Mater. (2015).
[11] D. Chicot, D. Mercier, F. Roudet, K. Silva, M.H. Staia, J. Lesage, J. Eur. Ceram. Soc. 27 (2007) 1905–1911.
[12] M. Dao, N. Chollacoop, K.J. Van Vliet, T.A. Venkatesh, S. Suresh, Acta Mater. 49 (2001) 3899–3918.
[13] D. Kiener, A.M. Minor, O. Anderoglu, Y.Q. Wang, S.A. Maloy, P. Hosemann, J. Mater. Res. 27 (2012) 2724–2736.
[14] P. Hosemann, C. Vieh, R.R. Greco, S. Kabra, J.A. Valdez, M.J. Cappiello, S.A. Maloy, J. Nucl. Mater. 389 (2009) 239–247.
[15] C. Heintze, F. Bergner, M. Hernandez-Mayoral, J. Nucl. Mater. 417 (2011) 980–983.
[16] C.D. Hardie, S.G. Roberts, J. Nucl. Mater. 433 (2013) 174–179.
[17] C.D. Hardie, S.G. Roberts, A.J. Bushby, J. Nucl. Mater. (2015)
[18] J.C. Gong, A. Wilkinson, Phil. Mag. Lett. 90 (2010) 503–512.
[19] D.E.J. Armstrong, A.J. Wilkinson, S.G. Roberts, J. Mater. Res. 24 (2009) 3268–3276.
[20] D. Kiener, C. Motz, G. Dehm, R. Pippan, Int. J. Mater. Res. 100 (2009) 1074–1087.
[21] D. Kiener, A.M. Minor, Nano Lett. 11 (2011) 3816–3820.
[22] J.C. Gong, A.J. Wilkinson, Acta Mater. 57 (2009) 5693–5705.
[23] M.D. Uchic, P.A. Shade, D.M. Dimiduk, JOM 61 (2009) 36–41.
[24] J.R. Greer, J.T.M. De Hosson, Prog. Mater. Sci. 56 (2011) 654–724.
[25] D.E.J. Armstrong, A.J. Wilkinson, S.G. Roberts, Phil. Mag. Lett. 91 (2011) 394–400.
[26] D. Di Maio, S.G. Roberts, J. Mater. Res. 20 (2005) 299–302.
[27] P.R. Howie, S. Korte, W.J. Clegg, J. Mater. Res. 27 (2012) 141–151.
[28] H. Dugdale, D.E.J. Armstrong, E. Tarleton, S.G. Roberts, S. Lozano-Perez, Acta Mater. 61 (2013) 4707–4713.
[29] D. Kiener, P. Hosemann, S.A. Maloy, A.M. Minor, Nat. Mater. 10 (2011) 608–613.
[30] E.M. Grieveson, D.E.J. Armstrong, S. Xu, S.G. Roberts, J. Nucl. Mater. 430 (2012) 119–124.
[31] Q. Guo, P. Landau, P. Hosemann, Y.Q. Wang, J.R. Greer, Small 9 (2013) 691–696.
[32] F.M. Halliday, D.E.J. Armstrong, J.D. Murphy, S.G. Roberts, Adv. Mater. Res. 59 (2009) 304–307.
[33] M. Rieth, S.L. Dudarev, S.M.G. de Vicente, J. Aktaa, T. Ahlgren, S. Autusch, D.E.J. Armstrong, M. Balden, N. Baluc, M.F. Barthe, W.W. Basuki, M. Battabyal, C.S. Becquart, D. Blagoeva, H. Boldyryeva, J. Brinkmann, M. Celino, L. Ciupinski, J.B. Correia, A. De Backer, C. Domain, E. Gaganidze, C. Garcia-Rosales, J. Gibson, M.R. Gilbert, S. Giusepponi, B. Gludovatzj, H. Greuner, K. Heinola, T. Hoschen, A. Hoffmann, N. Holstein, F. Koch, W. Krauss, H. Li, S. Lindig, J. Linke, C. Linsmeier, P. Lopez-Ruiz, H. Maier, J. Matejicek, T.P. Mishra, M. Muhammed, A. Munoz, M. Muzyk, K. Nordlund, D. Nguyen-Manh, J. Opschoor, N. Ordas, T. Palacios, G. Pintsuk, R. Pippan, J. Reiser, J. Riesch, S.G. Roberts, L. Romaner, M. Rosinski, M. Sanchez, W. Schulmeyer, H. Traxler, A. Urena, J.G. van der Laan, L. Veleva, S. Wahlberg, M. Walter, T. Weber, T. Weitkamp, S. Wurster, M.A. Yar, J.H. You, A. Zivelonghi, J. Nucl. Mater. 432 (2013) 482–500.
[34] P. Norajitra, S. Antusch, R. Giniyatulin, V. Kuznetsov, I. Mazul, H.J. Ritzhaupt-Kleissl, L. Spatafora, Fusion Eng. Des. 86 (2011) 1656–1659.
[35] S.J. Zinkle, N.M. Ghoniem, Fusion Eng. Des. 51–52 (2000) 55–71.
[36] M. Matijasevic, W. Van Renterghem, A. Almazouzi, Acta Mater. 57 (2009) 1577–1585.
[37] L. Malerba, G. Bonny, D. Terentyev, E.E. Zhurkin, M. Hou, K. Vortler, K. Nordlund, J. Nucl. Mater. 442 (2013) 486–498.
[38] A. Kohyama, A. Hishinuma, D.S. Gelles, R.L. Klueh, W. Dietz, K. Ehrlich, J. Nucl. Mater. 233 (1996) 138–147.
[39] J.F. Ziegler, M.D. Ziegler, J.P. Biersack, Nuclear instruments & methods in physics research section b-beam interactions with materials and atoms, 268 (2010) 1818–1823.
[40] G. Piazzesi, J. Phys. E Sci. Instrum. 6 (1973) 392–396.
[41] G. Simmons, H. Wang, Single Crystal Elastic Constants and Calculated Aggregate Properties: A Handbook, second ed., MIT Press, Cambridge, Mass., 1971.
[42] M. Madjasevic, A. Alrriazouzi, J. Nucl. Mater. 377 (2008) 147–154.
[43] D. Stork, P. Agostini, J.L. Boutard, D. Buckthorpe, E. Diegele, S.L. Dudarev, C. English, G. Federici, M.R. Gilbert, S. Gonzalez, A. Ibarra, C. Linsmeier, A. Li Puma, G. Marbach, P.F. Morris, L.W. Packer, B. Raj, M. Rieth, M.Q. Tran, D.J. Ward, S.J. Zinkle, J. Nucl. Mater. 455 (2014) 277–291.
[44] A. Giannattasio, Z. Yao, E. Tarleton, S.G. Roberts, Phil. Mag. 90 (2010) 3947–3959.
[45] A.J. Bushby, S.G. Roberts, C.D. Hardie, J. Mater. Res. 27 (2012) 85–90.
[46] D.E.J. Armstrong, P.D. Edmondson, S.G. Roberts, Appl. Phys. Lett. 102 (2013).